SCIENCE CHINA
Information Sciences

• **Supplementary File** •

Magnetic coupling governed pinning directions in magnetic tunnel junctions under magnetic field annealing with zero magnetic field cooling

Weibin Chen[1,3], Shaohua Yan[2,3], Zhiqiang Cao[2,3], Shiyang Lu[3], Xiaonan Zhao[1], Runrun Hao[2,3], Zitong Zhou[2,3], Zhi Li[2,3], Kun Zhang[2,3*], Shishen Yan[1*] & Qunwen Leng[1,2,3*]

[1]*School of Physics, State Key Laboratory of Crystal Materials, Shandong University, Jinan* 250100, *China;*
[2]*Fert Beijing Institute, MIIT Key Laboratory of Spintronics, School of Integrated Circuit Science and Engineering, Beihang University, Beijing* 100191, *China;*
[3]*Beihang-Georgtek Joint Microelectronics Institute, Qingdao Research Institute, Beihang University, Qingdao* 266101, *China*

Appendix A Film Stack Synthesis and Characterization

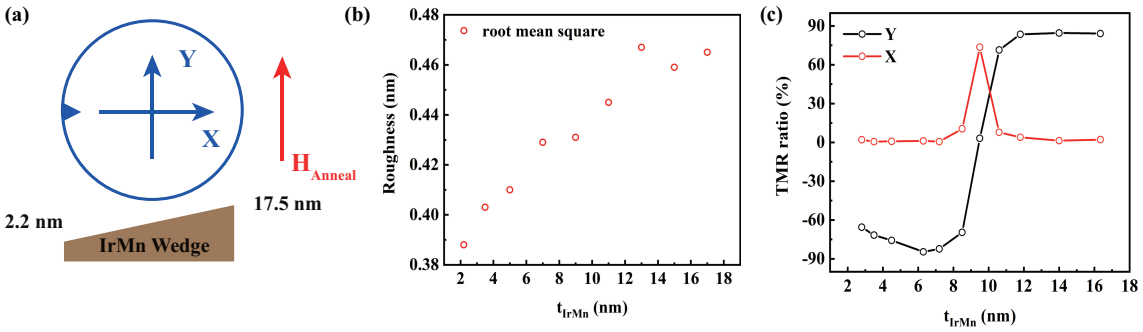

Figure A1 (a) Schematic for presenting variation trend of the IrMn thickness along the X direction and applied magnetic field (H_{Anneal}). (b) The root mean square (rms) of surface roughness dependence on the IrMn thickness. (c) The IrMn thickness dependent TMR ratio of membrane stack measured by CIPT with magnetic field sweeping along the X and Y axis.

A thin film stack with a structure of Ta (5) / CuN (20) / Ta (3) / CuN (20) / Ta (1.2) / $Ni_{47}Fe_{11}Cr_{42}$ (14) / $Ir_{20}Mn_{80}$ wedge / $Co_{70}Fe_{30}$ (2) (P1) / Ru (0.7) / [$Co_{70}Fe_{30}$ (0.5) / $CoFe_{60}B_{20}$ (1.8)] (P2) / MgO (1) / [$CoFe_{60}B_{20}$ (2) / Ta (0.25) / $NiFe_{19}$ (3.5)] (FL) / cap (the number is in unit of nm), as illustrated in the main text, is deposited on an 8-inch Si/SiO_2 substrate using a Singulus Rotaris magnetron sputtering system with a base pressure of $<4\times10^{-8}$ Torr. As shown in Figure A1(a), the wedgy IrMn layer is fabricated, with its thickness varying from 2.2 nm to 17.5 nm along the notch direction (X axis) by placing the substrate with an off-centered displacement relative to the center of the circular sputter source. In this case, the distance between the sputter source and substrate gradually decreases along the +X direction. Hence, the deposition rate of IrMn increases along the +X direction and a wedgy IrMn layer is fabricated. We also fabricate the wedgy IrMn single layer and perform atomic force microscopy characterization to study the relationship between the surface roughness and IrMn thickness. As summarized in Figure A1(b), with the increase of thickness from 2.2 nm to 17.5 nm, the root mean square (rms) of the surface roughness slightly augments from 0.378 nm to 0.465 nm, which meets the requirements of magnetic tunnel junction (MTJ) for flatness. In this MTJ stack, the bottom Ta (5) / CuN (20) / Ta (3) / CuN (20) layers and the top Ta (3) / CuN (5) / Ta (3) / Ru (3) cap layers are used as electrodes for current in-plane tunneling (CIPT) measurements. The Ta (1.2) /NiFeCr (14) seed layer can facilitate the growth of IrMn layer with (111) crystal orientation [1]. The bottom CoFe (2.0) pinned by the IrMn layer, is antiferromagnetically coupled with the top CoFe (0.5) / CoFeB (1.8) through the spacer layer Ru (0.7) to form the synthetic antiferromagnetic (SAF). Here, the CoFe (2.0) is defined as the pinned layer (P1), and the CoFe (0.5) / CoFeB (1.8) is defined as the pinned layer 2 (P2) (or so-called the fixed layer). And the CoFeB (2.0) is ferromagnetically coupled with the soft magnetic layer of NiFe (3.5) by the spacer layer Ta (0.25) to form the free layer (FL). It is notable that the interlayer coupling between the free layer and fixed layer is ferromagnetic in this stack [2,3]. Next, the films are annealed in a high-vacuum chamber at 270°C under a magnetic field of 10 kOe (H_{Anneal}) along the +Y direction for 1 h. Then, the magnetic field is removed during the cooling process.

Figure A1(c) shows tunneling magnetoresistance (TMR) ratio are the functions of the IrMn thickness (t_{IrMn}). Here, the TMR ratio is always defined as $\frac{R_{H+}-R_{H-}}{MIN(R_{H+},R_{H-})}\times100\%$, where R_{H+} and R_{H-} are the measured sheet resistance under the positive and negative saturation magnetic field, respectively. And the sweeping direction of magnetic field is same for all points. The function

* Corresponding author (email: zhang_kun@buaa.edu.cn, shishenyan@sdu.edu.cn, lengqw@bhqditi.com)

of "MIN(A,B)" represents the smaller one in A and B. With the magnetic field sweeping along the Y axis, the sign of the TMR ratio switches from negative to positive with the increasing IrMn thickness. The "mutation" occurred at the 9.5 nm point where the TMR ratio is almost zero. Meanwhile, the TMR ratio is also obtained for the sample with 9.5 nm IrMn with the magnetic field sweeping along the X axis. From these results, we can find the pinning direction of the MTJ changes with the increasing IrMn thickness.

Appendix B Magnetic and Magnetoresistance Proterties of MTJs

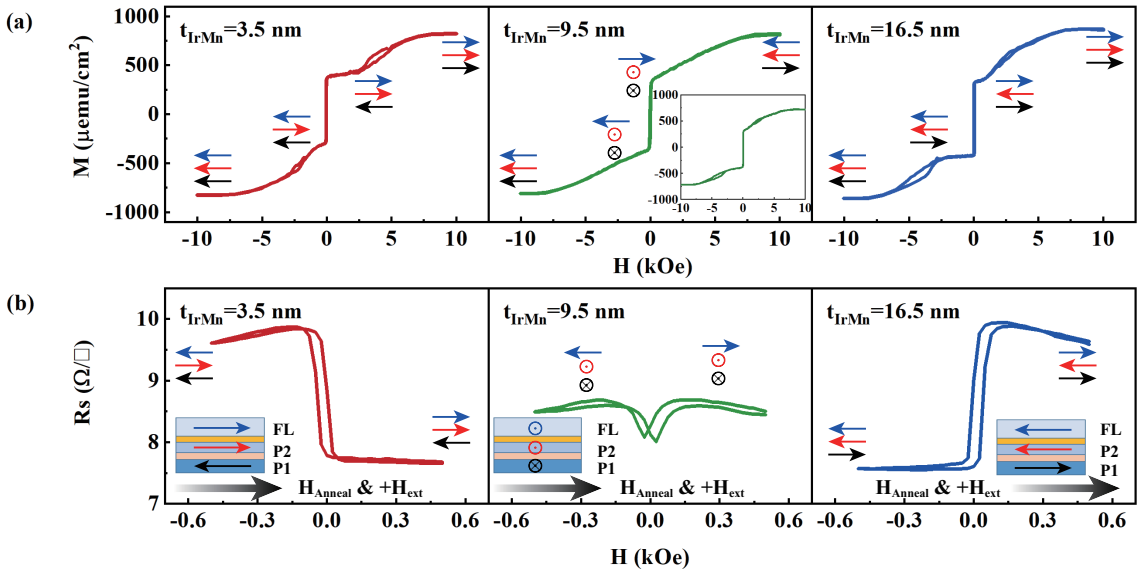

Figure B1 (a) The M−H loop and (b) R_s−H loop of the membrane stack with different IrMn thickness under the magnetic field sweeping along the Y axis. The inset of (a) is M−H loop for the sample with 9.5 nm IrMn under the magnetic field sweeping along the X axis. The inset of (b) is the final state of P1, P2 and free layer after the zero magnetic field cooling treatment.

Figure B1(a) presents the magnetic hysteresis (M−H) curves of the MTJ stack with various IrMn thicknesses with the magnetic field sweeping along the Y axis. For the sample with t_{IrMn}=3.5 nm, the remarkable small hysteresis loop under the magnetic field from 2.5 kOe to 5 kOe clearly represents that the pinning direction of the pinned layer is along the −Y direction (antiparallel to the direction of H_{Anneal}). Meanwhile, the inverted M−H curve for samples with t_{IrMn}=16.5 nm indicates that the pinning direction of the pinned layer is flipped by 180°. As a contrast, there is no small hysteresis loop observed for the sample with t_{IrMn}=9.5 nm, indicating that the pinning direction is perpendicular to the direction of H_{Anneal}. To confirm this point, we measure its M−H curve with the magnetic field sweeping along the X axis, as shown in the inset of Figure B1(a), in which the remarkable small hysteresis loop is observed. The magnetic field dependent sheet resistance (R_s−H) loop measured by sweeping magnetic fields from −0.5 kOe to 0.5 kOe along the Y axis is shown in Figure B1(b). In this case, only the magnetization of free layer changes with the applied magnetic field while the magnetization of P2 is fixed. For the samples with t_{IrMn}=3.5 nm and t_{IrMn}=16.5 nm, opposite R_s−H curves are observed, indicating their inverse the pinning direction. Meanwhile, only a minor difference in resistance is observed for the sample with t_{IrMn}=9.5 nm because of the X direction pinning. These behaviors of observed R_s−H curves are consistent with the TMR ratio results, as shown in Figure A1(c).

Appendix C Theoretical Simulation

Under the zero magnetic field cooling process, the Zeeman energy disappears. Hence, the considerable energy in the model includes the interlayer coupling energy (E_{in}) between free layer and P2, antiferromagnetic (AFM) coupling energy (E_{SAF}) between P1 and P2, and exchange bias coupling energy (E_{ex}) between IrMn layer and P1. The total energy per unit area (E_{total}) is written as

$$E_{total} = E_{in} + E_{SAF} + E_{ex} \tag{C1}$$

Schematic geometry of the magnetization M of each layer is illustrated in Figure C1(a). M_{P1}, M_{P2} and M_{FL} are the magnetization of P1, P2 and free layer, respectively. θ_{P1}, θ_{P2}, θ_{FL} are the angles between M_{P1}, M_{P2}, M_{FL} and the direction of H_{Anneal}, respectively. The E_{in} is expressed as below

$$E_{in} = [-H_{in}M_{P2}t_{P2}M_{FL}t_{FL}/(M_{P2}t_{P2} + M_{FL}t_{FL})]\cos(\theta_{FL} - \theta_{P2}) \tag{C2}$$

where H_{in} is the interlayer coupling field, t_{P1}, t_{P2} and t_{FL} are the thickness of P1 and P2 and free layer. The E_{SAF} can be expressed by

$$E_{SAF} = [H_{SAF}M_{P1}t_{P1}M_{P2}t_{P2}/(M_{P1}t_{P1} + M_{P2}t_{P2})]\cos(\theta_{P2} - \theta_{P1}) \tag{C3}$$

where H_{SAF} is the AFM coupling field between P1 and P2. And the E_{ex} can be described by the following expression

$$E_{ex} = -M_{P1}t_{P1}H_{ex}\cos\theta_{P1} \tag{C4}$$

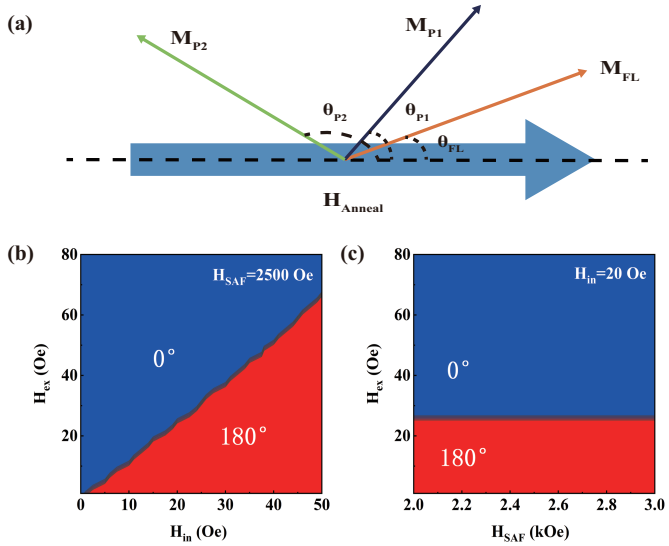

Figure C1 (a) Schematic geometry of the magnetization of P1, P2 and free layer. (b) The magnetization direction of P1 (i.e., the pinning direction) as a function of H_{ex} and H_{in} with H_{SAF}=2500 Oe. (c) The magnetization direction of P1 as a function of H_{ex} and H_{SAF} with H_{in}=20 Oe.

where H_{ex} is the exchange bias field.

At first, because the Curie temperature of CoFe and CoFeB is high up to 1000°C [4,5], which is much higher than the annealing temperature of 270°C. The values of M_{P1}, M_{P2} and M_{FL} remain nearly unchanged during the annealing treatment. Therefore, the related parameters are measured by superconducting quantum interference device (SQUID) at room temperature, i.e., $M_{P1}t_{P1}=5.05\times10^{-4}$ emu/cm^2, $M_{P2}t_{P2}=6.47\times10^{-4}$ emu/cm^2 and $M_{FL}t_{FL}=8.09\times10^{-4}$ emu/cm^2. Moreover, the coupling strengths of H_{in} and H_{SAF} are also based on the Curie temperature of CoFe and CoFeB, which also remain nearly unchanged during the annealing treatment, so the values of H_{in} and H_{SAF} are set to the ranges of 0 Oe to 50 Oe and 2.5 kOe to 3 kOe during the theoretical calculation. At last, the value of H_{ex} is related to the AFM order of IrMn, so it is strongly affected by the AFM film thickness and decreases sharply near the blocking temperature [6]. Because the annealing temperature is close to the blocking temperature of IrMn, we set the range of H_{ex} to be 0 Oe to 80 Oe.

According to the minimum energy principle, we can determine the stable states (i.e., the final orientation) of P1, P2 and free layer. Figure C1(b) exhibits the dependence of magnetization evolution of P1 (i.e., the pinning direction of MTJs) on H_{ex} and H_{in} with fixed H_{SAF}=2500 Oe. A clear boundary separates the final states of P1, where the E_{ex} and E_{in} cancel each other out. With the increasing H_{in}, the required H_{ex} to set the magnetization direction of P1 along H_{Anneal} also enlarges, demonstrating their competing relationship. When $E_{ex}>E_{in}$ ($E_{ex}<E_{in}$), the magnetization of P1 will be along (opposite) with the direction of H_{Anneal}. The impact of H_{SAF} on the pinning direction has also been considered, as shown in Figure C1(c). The magnetization of P1 flip at the same H_{ex} for H_{SAF} ranging from 2 kOe to 3 kOe with fixed H_{in}=20 Oe, which means that the AFM coupling of SAF only works as a bound between the interlayer coupling and exchange bias coupling, and doesn't directly determine the final states. The simulation results further verify that the competition between E_{ex} and E_{in} is responsible for aligning the pinning direction in MTJs under the zero magnetic field cooling process.

Appendix D Experimental Verification

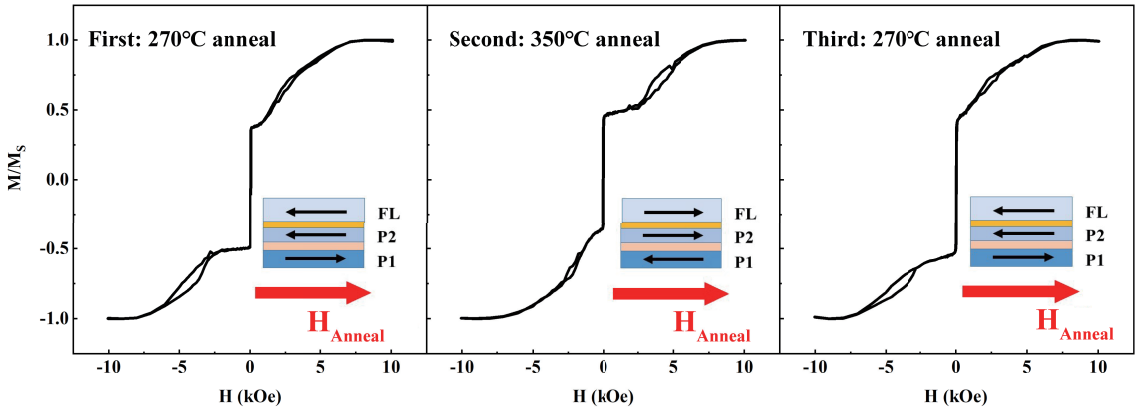

Figure D1 Normalized M−H loop of the sample with 16.5 nm IrMn after three consecutive zero magnetic field cooling process with annealing temperature 270°C to 350°Cand back to 270°C. The inset shows the direction of H_{Anneal} and the final direction of P1, P2 and free layer in this case.

A control experiment is designed to verify the proposed competing mechanism. We anneal a film stack with 16.5 nm IrMn three times under the zero magnetic field cooling process: 270°C with H_{Anneal}=10 kOe, then 350°C with H_{Anneal}=10 kOe, and finally back to 270°C with H_{Anneal}=10 kOe. Figure D1 shows the normalized M−H curve of this sample, we successfully manipulate the pinning direction by the controlling annealing temperature. The reason is discussed in the following. The blocking temperature for the 16.5 nm IrMn is higher than 270°C and lower than 350°C [7]. Therefore, the pinning direction is along the direction of H_{Anneal} at the first 270°C anneal because of $E_{ex}>E_{in}$. For the 350°C treatment, the pinning direction is antiparallel to the direction of H_{Anneal} because of $E_{ex}<E_{in}$. Finally, when the film stack is annealed at 270°C again, the applied H_{Anneal} can destroy the previous H_{ex} and the pinning direction is back to the direction of H_{Anneal} because of $E_{ex}>E_{in}$.

References

1 Devasahayam A J, Sides P J, Kryder M H. Magnetic, temperature, and corrosion properties of the NiFe/IrMn exchange couple. J. Appl. Phys., 1998, 83: 7216

2 Platt C, McCartney M. Magnetic interlayer coupling in ferromagnet/insulator/ferromagnet structures. Phys. Rev. B, 2000, 61: 9633-9641

3 Li K, Wu Y, Qiu J, et al. Suppression of interlayer coupling and enhancement of magnetoresistant in spin valves with oxide layer. Appl. Phys. Lett., 2001, 79: 3663-3665

4 Heyne L, Kläui M, Backes D, et al. Direct imaging of current-induced domain wall motion in CoFeB structures. J. Appl. Phys., 2008, 103: 07D928

5 Rohman L, Arkundato A, Mulyani Y T, et al. Magnetic susceptibility and curie temperature of $Co_{1-x}Fe_x$ alloy nanocube and nanosphere using micromagnetic simulation. J. Phys. Conf. Ser., 2021, 1825: 012003

6 Fuke H N, Saito K, Yoshikawa M, et al. Influence of crystal structure and oxygen content on exchange-coupling properties of IrMn/CoFe spin-valve films. Appl. Phys. Lett., 1999, 75: 3680-3682

7 Devasahayam A J, Sides P J, Kryder M H. Magnetic, temperature, and corrosion properties of the NiFe/IrMn exchange couple. J. Appl. Phys., 1998, 83: 7216